Superconducting nanowire photon-number-resolving detector at telecommunication wavelengths

ALEKSANDER DIVOCHIY[1], FRANCESCO MARSILI[2*†], DAVID BITAULD[2†], ALESSANDRO GAGGERO[3], ROBERTO LEONI[3], FRANCESCO MATTIOLI[3], ALEXANDER KORNEEV[1], VITALIY SELEZNEV[1], NATALIYA KAUROVA[1], OLGA MINAEVA[1], GREGORY GOL'TSMAN[1], KONSTANTINOS G. LAGOUDAKIS[2], MOUSHAB BENKHAOUL[4], FRANCIS LÉVY[4] AND ANDREA FIORE[2†]

[1]Department of Physics, Moscow State Pedagogical University (MSPU), 119992 Moscow, Russian Federation
[2]Institute of Photonics and Quantum Electronics (IPEQ), Ecole Polytechnique Fédérale de Lausanne (EPFL), Station 3, CH-1015 Lausanne, Switzerland
[3]Istituto di Fotonica e Nanotecnologie (IFN), CNR, via Cineto Romano 42, 00156 Rome, Italy
[4]Institute of Complex Matter Physics (IPMC), Ecole Polytechnique Fédérale de Lausanne (EPFL), Station 3, CH-1015 Lausanne, Switzerland
*e-mail: francesco.marsili@epfl.ch
†Present address: COBRA Research Institute, Eindhoven University of Technology, PO Box 513, NL-5600MB Eindhoven, The Netherlands

Published online: 13 April 2008; doi:10.1038/nphoton.2008.51

Optical-to-electrical conversion, which is the basis of the operation of optical detectors, can be linear or nonlinear. When high sensitivities are needed, single-photon detectors are used, which operate in a strongly nonlinear mode, their response being independent of the number of detected photons. However, photon-number-resolving detectors are needed, particularly in quantum optics, where *n*-photon states are routinely produced. In quantum communication and quantum information processing, the photon-number-resolving functionality is key to many protocols, such as the implementation of quantum repeaters[1] and linear-optics quantum computing[2]. A linear detector with single-photon sensitivity can also be used for measuring a temporal waveform at extremely low light levels, such as in long-distance optical communications, fluorescence spectroscopy and optical time-domain reflectometry. We demonstrate here a photon-number-resolving detector based on parallel superconducting nanowires and capable of counting up to four photons at telecommunication wavelengths, with an ultralow dark count rate and high counting frequency.

Among the approaches proposed so far for photon-number-resolving (PNR) detection (Table 1) are detectors based on charge integration or field-effect transistors[3–5], which are, however, affected by long integration times, leading to bandwidths of <1 MHz. Transition edge sensors[6] operate at 100 mK and show long response times (several microseconds). Approaches based on photomultipliers[7] and avalanche photodiodes, such as the visible-light photon counter[8,9], two-dimensional arrays of avalanche photodiodes[10,11] and time-multiplexed detectors[12,13] are not sensitive or are plagued by high dark count rates (DKs) and long dead times in the telecommunication spectral windows. Arrays of single-photon detectors (SPDs) also involve complex readout schemes[11] or separate contacts, amplification and discrimination[14]. The parallel nanowire detector (PND) presented here significantly outperforms these approaches in terms of simplicity, sensitivity, speed and multiplication noise.

The basic structure of the PND comprises the parallel connection of N superconducting nanowires, each connected in series to a resistor R_0 (Fig. 1). The detecting element is a few nanometres thick, and is composed of a NbN wire about 100 nm wide folded in a meander pattern. Each branch acts as a superconducting single-photon detector[15] (SSPD). If a superconducting nanowire is biased close to its critical current, the absorption of a photon causes the formation of a non-superconducting barrier across its cross-section, and the bias current is pushed to the external circuit. In the parallel configuration proposed here, the currents from different wires can sum up on the external load, producing an output voltage pulse proportional to the number of photons. The time evolution of the device after photon absorption can be simulated using the equivalent circuit of Fig. 1b. Let $I^{(i)} = I_B = V_B/R_0$ be the current flowing through the ith branch when the device is biased with a voltage source V_B. If a photon reaches the ith nanowire, it will cause the superconducting–normal transition with a probability $\eta_i = \eta(I_B/I_C^{(i)})$, where η is the current-dependent quantum efficiency and $I_C^{(i)}$ is the critical current of the nanowire[14]. Because of the sudden increase in the resistance of the nanowire, its current is then redistributed between the other $N-1$ branches and the input resistance of the amplifier $R_A = 50\ \Omega$, (Fig. 2a,b). The device demonstrates PNR capability if the leakage current drained by each of the still superconducting nanowires, δI_{lk}, is negligible ($\delta I_{lk} \ll I_B$). The leakage current is also undesirable, because it lowers the signal available for amplification and temporarily increases the values of $I^{(i)}$, eventually driving other nanowires into a non-superconducting state. It can be reduced by engineering the dimensions of the nanowire (thus its kinetic inductance[16]) and of the bias resistor to maximize the wire impedance Z_B while keeping a stable

Table 1 Reported performance for detectors with PNR functionality.

	Repetition rate (Hz)	DK (Hz)	η (%)	NEP (W Hz$^{-1/2}$)	λ (nm)	M_{noise}	M_{max}	T (K)	Readout
CIPD (ref. 3)	40	NR	80	NR	1,550	Yes	NR	4.2	Cryo JFET
QD-FET (refs 4,5)	2×10^5	0.4	1.3	2×10^{-17}	684	Yes	3	4.2	Cryo MESFET
TES (ref. 6*)	5×10^4	400	89	4×10^{-18}	1,550	Yes	11	<0.1	SQUID array
PMT (ref. 7)	6.7×10^5	400	7	1×10^{-16}	523	Yes	9	Room T	Room T amp.
VLPC (refs 8,9)	1.5×10^4	2×10^4	85	9×10^{-17}	543	Yes	10	6–7	Cryo preamp.
MPPC (ref. 10)	1×10^4	1.4×10^5	25–65	7×10^{-16}	400	Yes	100–1,600	Room T	Room T amp.
APD array[11]	2×10^4	1.6×10^8	33	1×10^{-14}	1,064	No	1,024	246	Multichannel
Time multiplexed[12,24]	1×10^4	NR	66	NR	700–800	No	8–16	Room T	Two-channel
PND	8×10^7	0.15	2	4×10^{-18}	1,300	No	4	2	Room T amp.

CIPD, charge integration photodiode, QD-FET, quantum dot field-effect transistor; TES, transition edge sensor; PMT, photomultiplier; VLPC, visible-light photon counter; MPPC, multi-pixel photon counter; APD, avalanche photodiode; λ, optical excitation wavelength; M_{noise}, device affected by multiplication noise; M_{max}, maximum number of detected photons; NR, not reported; Cryo JFET: cryogenic junction gate field-effect transistor; Cryo MESFET: cryogenic metal epitaxial semiconductor field-effect transistor; SQUID: superconducting quantum interference device; amp.: amplifier; preamp.: preamplifier.
Repetition stands for the repetition frequency used in reported experiments (does not necessarily represent the maximum possible rate).
*A better NEP (1×10^{-19} W Hz$^{-1/2}$), with a lower quantum efficiency ($\eta = 20\%$) was reported in ref. 25.

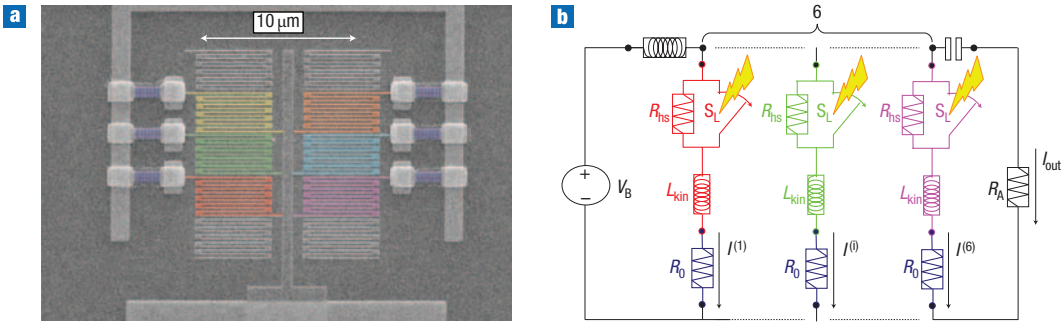

Figure 1 The parallel nanowire detector (PND). a, A scanning electron microscopy image of a 10×10 μm^2 6-PND fabricated on MgO. The nanowire width is $w = 100$ nm and the fill factor is $f = 40\%$. The active nanowires (in colour) are connected in series with Au–Pd resistors (in blue). The floating meanders at the corners of the active area correct for the proximity effect. **b**, Equivalent circuit of the 6-PND. The superconducting nanowire is modelled as the series of an inductance L_{kin} accounting for its kinetic inductance, a switch S_L that opens on the hot-spot resistance $R_{hs} \sim 1$ kΩ, simulating the absorption of a photon.

bias condition and a short response time. A design without bias resistors is also possible. It simplifies the fabrication process, but, as Z_B is lower, δI_{lk} significantly limits the maximum bias current allowed for the stable operation of the device and thus its quantum efficiency.

The PNDs were fabricated on ultrathin NbN films (4 nm) on MgO (ref. 17) and R-plane sapphire[18] using electron-beam lithography and reactive-ion etching (see Methods). Designs with and without the integrated bias resistors were tested. A scanning electron microscope image of a PND with six parallel wires (6-PND) and series resistors fabricated on MgO is shown in Fig. 1a.

The photoresponse of a 10×10 μm^2 4-PND probed with light at 1.3 μm was recorded by a sampling oscilloscope (inset of Fig. 2c). All four possible amplitudes can be observed. The pulses show a full-width at half-maximum as low as 660 ps. The PNDs showed counting performance when probed with light at repetition rates of 26 MHz and 80 MHz (Fig. 2c and inset of Fig. 4a, respectively), outperforming any existing PNR detector at telecommunication wavelengths by three orders of magnitude. Indeed, PNDs have by design a reduced recovery time (by a factor N^2) even compared with traditional SSPDs, owing to their reduced kinetic inductance[19].

To prove the PNR capability of the PND, we measured the photocount statistics. The photon-number probability distribution, $Q(n)$, measured with a PNR detector is related to the incoming distribution $S(m)$ by the relation: $Q(n) = \sum_{m \geq n} P(n|m) \cdot S(m)$, where $P(n|m)$ is the probability that n photons are detected when m are sent to the device. Under illumination with a weak poissonian light source (see equation (4) in the Methods), the probability $Q(1)$ of detecting one photon is proportional to the mean photon number μ, $Q(2)$ is proportional to μ^2, and so on. A 5-PND was tested with coherent light from an 850-nm GaAs pulsed laser. In Fig. 3a the detection probabilities relative to one-, two- and three-photon absorption events are plotted for μ varying over two orders of magnitude. As predicted by equation (4), $Q(n) \propto \mu^n$, which demonstrates the PNR functionality. The one-photon quantum efficiency η at 1.3 μm and DK were measured as a function of bias current (Fig. 3b). The lowest DK value measured was 0.15 Hz for $\eta = 2\%$ (yielding a noise equivalent power (NEP) (ref. 20) of 4.2×10^{-18} W Hz$^{-1/2}$), limited only by the room-temperature background radiation coupling to the PND.

The typical application of a PNR detector is the reconstruction of an unknown photon-number distribution $S(m)$, which can be recovered given $Q(n)$ and the matrix of the conditional probabilities[21] $P^N = [P^N_{n,m}]$ (where $P^N_{n,m} = P^N(n|m)$ for an N-PND). Considering equations (1) to (3) in the Methods, it is clear that P^N can be calculated if the vector of the N different quantum efficiencies $\bar{\eta} = [\eta_i]$ is known. $\bar{\eta}$ can be determined by fitting the $Q(n)$ measured when probing the device with a light whose $S(m)$ is known. A 5-PND was tested with the coherent emission from a Ti:sapphire laser. To determine $Q(n)$, histograms of the photoresponse voltage peak V_{pk} were built for values of μ ranging from ~1 to ~100 (Fig. 4). The experimental probability

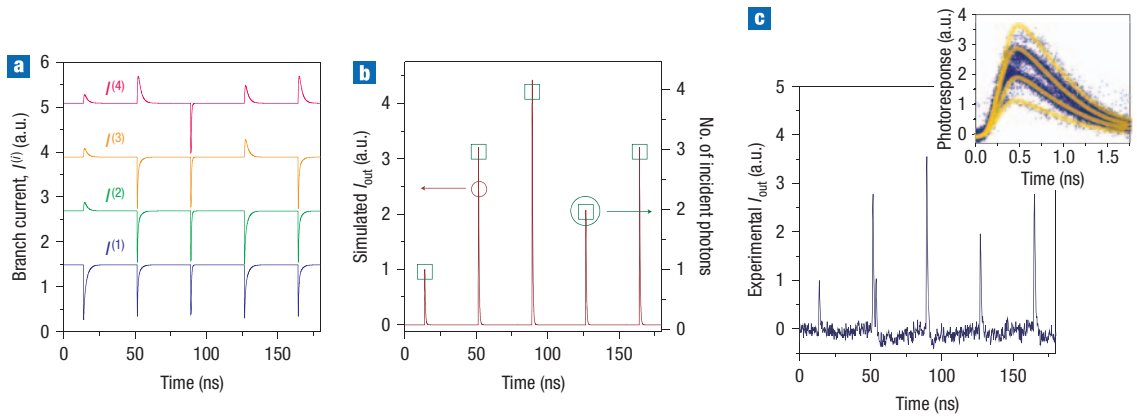

Figure 2 The PND photoresponse. a, Simulated $I^{(i)}$ for a 4-PND with $\eta_i = 1$. The curves are shifted vertically for clarity. **b**, Simulated I_{out} (continuous curve), and number of photons in each light pulse (open squares). The photons are never absorbed on the same nanowire. **c**, Single-shot oscilloscope trace of a $10 \times 10\ \mu m^2$ 4-PND (with integrated bias resistors) probed in the cryogenic probe station under illumination with 1.3 μm, 100-ps pulses from a laser diode. The average photon number per pulse was 1.5×10^4. Inset: Photoresponse transients taken with a 40-GHz sampling oscilloscope. The orange solid curves are guides to the eye.

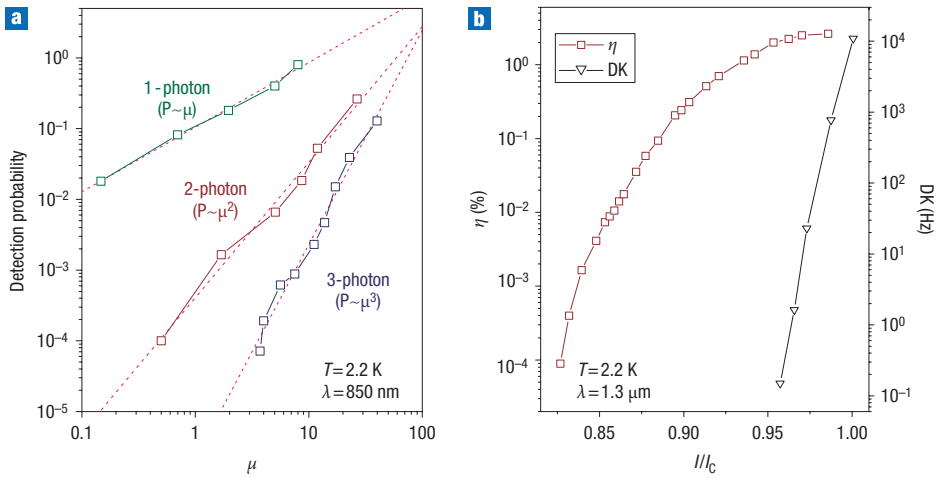

Figure 3 The probability of *n*-photon detection versus incoming mean photon number. A 5-PND (with integrated bias resistors) was tested under uniform illumination in a liquid He bath (temperature, $T = 2.2$ K). **a**, Detection probabilities relative to the one- (green open squares), two- (red open squares) and three-photon (blue open squares) absorption events as a function of μ. The light pulses at 0.85 μm from the GaAs pulsed laser were 30 ps wide. The photoresponse from the device was sent to the counter. As η is a few per cent and μ is a few tens, equation (4) is valid. **b**, Quantum efficiency (red open squares) at 1.3 μm and DK (black open triangles) versus bias current.

distribution $Q(n)$ measured for different μ was then fitted to the one predicted by the model (see Methods) using the vector $\bar{\eta}$ as the free parameter (Fig. 5). The photocount statistics of six levels is well fitted over almost two orders of magnitude of mean photon number, confirming the validity of the model. Additionally, the fitted efficiencies (inset of Fig. 5) are rather uniform, indicating a high-quality fabrication process.

Several effects may limit the counting capability M_{max} of a PNR detector. One is the quantum efficiency. From equation (2) in the Methods, assuming the detector saturation is negligible ($n \ll N$) and that all the branches are equal ($\eta_i = \eta$), the probability $Q(n)$ of detecting n photons is proportional to η^n. In the PND tested, $\eta \sim 2\%$ at 1.3 μm, which we attribute to non-optimum film thickness and device design; this obviously prevents the application of the present device to n-photon states measurement for $n \gg 1$. Nevertheless, the η of SPDs based on the same detection mechanism can be increased to ~60% (ref. 22), and could potentially exceed 90% using optimized optical cavities. Indeed, we are presently working on the integration of the PND on epitaxial GaAs/AlAs Bragg mirrors. We also stress that uniform illumination of the wires is needed to achieve optimum performance. The second limitation is electrical noise. Pulse height discrimination can be performed as long as the noise remains lower than the one-photon signal amplitude. In most PNR detectors[3–10] the noise increases with detection level due to multiplication noise, which limits the maximum number of resolvable photons. In contrast, no multiplication noise is seen in PNDs, as the width of the histogram peaks is independent of the number of detected photons n (Fig. 4). Indeed we expect an excess noise factor (F) (ref. 23) close to unity in the PND,

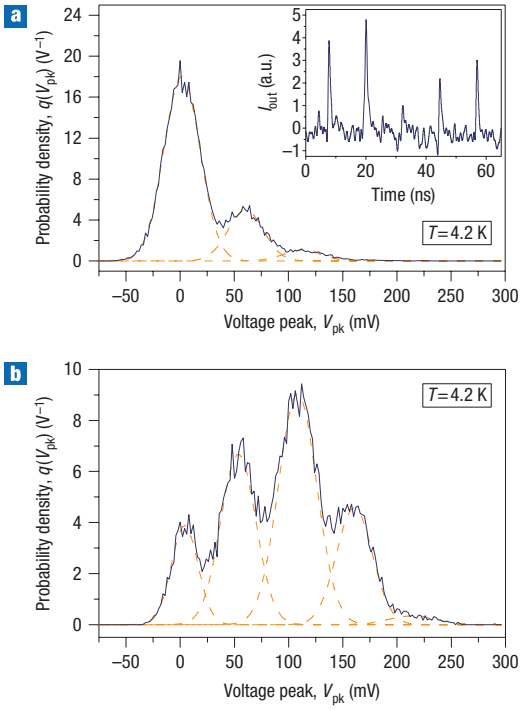

Figure 4 Histograms of the photoresponse voltage peak. a, **b**, An 8.6 × 8 μm^2 5-PND (with no integrated bias resistors) was tested under uniform illumination at T = 4.2 K (with μ = 7.7 (**a**) and 64.9 (**b**)). The light pulses at 700 nm from a Ti:sapphire laser were 40 ps wide (after propagation in the optical fibre) and the repetition rate was 80 MHz. The signal from the device was sent to the 1-GHz oscilloscope. The photoresponse was sampled for a gate time of 5 ps, making the dark counts negligible. The solid lines are the experimental histograms and the dashed lines represent the fit. Inset: Single-shot oscilloscope trace during photodetection at 80 MHz repetition rate.

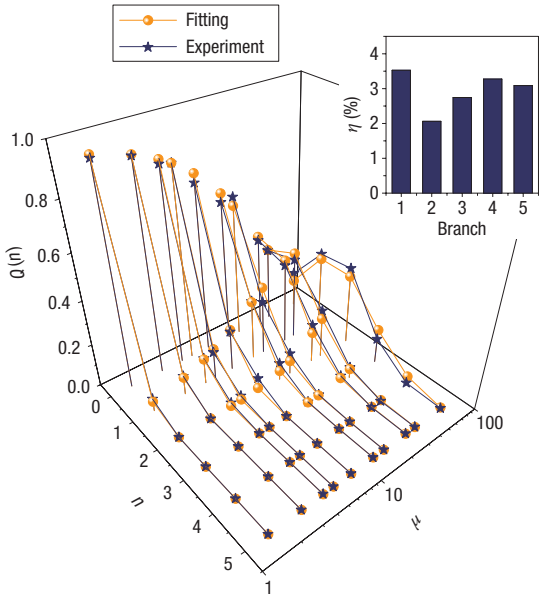

Figure 5 Experimental probability distribution versus mean photon number. The experimental discrete probability distribution $Q(n)$ (filled stars) was estimated from the continuous probability density $q(V_{pk})$ (Fig. 4) fitting the histograms to the sum of six gaussian distributions and calculating their area. The 5-PND was probed with several incident mean photon numbers μ: 1.5, 2.8, 4.3, 5.3, 7.7, 12.5, 15.9, 26.9, 33.6, 64.9. The experimental values for $Q(n)$ were then fitted (orange circles) using a genetic algorithm to recover $\bar{\eta}$. Inset: Reconstructed quantum efficiency vector. The standard deviation is 20% of the mean value, proof of the excellent uniformity of the device.

because the noisy quasi-particle multiplication process[24] causes a fluctuation only in the hot-spot resistance (∼1 kΩ) and not in the output current. The output current is determined by the partition with the much lower load resistance R_A. A third limitation to M_{max} in PNDs is the leakage current δI_{lk}, which restricts the number of parallel wires. However, this issue can be overcome by switching from voltage to current readout (for example, by using a transimpedance amplifier), thus decreasing the load impedance.

In conclusion, a new PNR detector, the parallel nanowire detector, has been demonstrated that significantly outperforms existing approaches in terms of sensitivity, speed and multiplication noise in the telecommunication wavelength range. In particular (Table 1), it provides a repetition rate (80 MHz) three orders of magnitude larger than any existing detector at telecommunication wavelengths[3,6,11] and a sensitivity (NEP = 4.2 × 10^{-18} W Hz$^{-1/2}$) between one and two orders of magnitude better, with the exception of transition edge sensors[6], which require a much lower operating temperature. The high repetition rate and high sensitivity make it suitable—for the first time—for replacing correlation set-ups in quantum optics experiments at telecommunication wavelengths. Compared with SPD arrays[14], this approach allows a much simpler readout and is thus scalable to the measurement of photon numbers greater than two. Indeed, by increasing the efficiency, the performance needed for the single-shot measurement of photon number, as needed in many quantum communication and computing protocols, can be reached. Finally, increasing the maximum photon number to 20–30 photons, the PND could be used as an 'analog' detector with single-photon sensitivity, bridging the gap between conventional and single-photon detectors.

METHODS

FABRICATION

Films of NbN 3–4 nm thick were grown on sapphire (substrate temperature T_S = 900 °C) or MgO (T_S = 400 °C) substrates by reactive magnetron sputtering in an argon–nitrogen gas mixture. Using an optimized sputtering technique, our NbN films of thickness 40 Å exhibited a superconducting transition temperature of 10.5 K and a superconducting transition width of 0.3 K.

Detector size ranged from 5 × 5 μm^2 to 10 × 10 μm^2, with the number of parallel branches varying from 4 to 14. The nanowires were 100 to 120 nm wide and the fill factor of the meander was 40–60%. The length of each nanowire ranged from 25 to 100 μm. For the devices on MgO, the three nanolithography steps needed to fabricate the structure were carried out by using a field-emission gun electron-beam lithography system (acceleration voltage 100 kV). In the first step, pads and alignment markers (60 nm gold on 10 nm titanium) were fabricated by lift-off using a polymethylmethacrylate (PMMA) stencil mask. In the second step, a hydrogen silsesquioxane (HSQ) mask was defined, reproducing the meander pattern. All the unwanted material, that is, the material not covered by the HSQ mask and the Ti/Au film, was removed by using fluorine-based reactive-ion etching. Finally, with the third step the bias resistors (85-nm AuPd alloy) aligned with the two previous layers were fabricated by lift-off using a PMMA stencil mask.

Details of the fabrication process for the devices on sapphire can be found in ref. 20.

MEASUREMENT SET-UP

Electro–optical characterizations were performed in a cryogenic probe station with an optical window and in cryogenic dipsticks. Bias current was supplied through the d.c. port of a bias-T by a low-noise voltage source in series with a

bias resistor. The a.c. port of the bias-T was connected to high-bandwidth, low-noise amplifiers. The amplified signal was fed to a 1-GHz-bandwidth single-shot oscilloscope, a 40-GHz-bandwidth sampling oscilloscope or a 150-MHz counter. The optical input was provided by a fibre-pigtailed, gain-switched laser diode at a wavelength of 1.3 μm, a mode-lock Ti:sapphire laser at a wavelength of 700 nm or an 850-nm GaAs pulsed laser. Throughout the paper, the efficiency η is defined with respect to the photon flux incident on the device area, typically $10 \times 10\ \mu m^2$.

In the cryogenic probe station the devices were tested at a temperature $T = 5$ K. The light was fed to the PNDs through a single-mode optical fibre coupled with a long-working-distance objective, allowing the illumination of a single detector.

In the cryogenic dipsticks the devices were tested at 4.2 K or 2 K. The light was sent through a single-mode optical fibre, either put in direct contact and aligned with the active area of a single device or coupled with a short focal length lens, placed far from the plane of the chip to ensure uniform illumination.

DERIVATION OF THE CONDITIONAL PROBABILITIES

Assuming that the illumination of the device is uniform, the parallel connection of N nanowires is equivalent to a balanced lossless N-port beam splitter, with every channel terminating with an SPD. Each incoming photon then has an equal probability of reaching one of the N SPDs. Each SPD can detect a photon with a probability η_i $(i = 1, \ldots, N)$ different from all the others, and gives the same response for any number $(m \geq 1)$ of photons detected. Following ref. 14, two classes of terms in P^N can be calculated directly, the others being derived from these by a recursion relation. These terms are the probabilities $P^N_{m,m}$ that all the $m \leq N$ photons sent are detected and $P^N_{0,m}$ that no photons are detected when m are sent. In the case of zero detections, $P^N_{0,m}$ is given by

$$P^N_{0,m} = \sum_{i_1=1,\ldots,i_m=1}^{N} \left[\frac{1-\eta_{i_1}}{N} \times \cdots \times \frac{1-\eta_{i_m}}{N}\right] \tag{1}$$

For the case where all the photons are detected, because m photons must reach m distinct nanowires,

$$P^N_{m,m} = \sum_{\substack{i_1=1,\ldots,i_m=1 \\ i_p \neq i_q \text{ for } p \neq q}}^{N} \left[\frac{\eta_{i_1}}{N} \times \cdots \times \frac{\eta_{i_m}}{N}\right] \quad \text{for } m \leq N \tag{2}$$

The recursion relation for P^N_{nm} is

$$P^N_{n,m} = P^N_{n,m-1}\left[\frac{n}{N} + \frac{n!}{N!} \times \sum_{\substack{i_1=1,\ldots,i_{N-n}=1 \\ i_p \neq i_q \text{ for } p \neq q}}^{N} \left(\frac{1-\eta_{i_1}}{N} + \cdots + \frac{1-\eta_{i_{N-n}}}{N}\right)\right] + P^N_{n-1,m-1}\left[\frac{(n-1)!}{N!} \times \sum_{\substack{i_1=1,\ldots,i_{N-(n-1)}=1 \\ i_p \neq i_q \text{ for } p \neq q}}^{N} \left(\frac{1-\eta_{i_1}}{N} + \cdots + \frac{1-\eta_{i_{N-(n-1)}}}{N}\right)\right] \tag{3}$$

The first term on the right-hand side of equation (3) is the probability that n photons are detected when $m-1$ are sent, times the probability that the mth photon reaches one of the n nanowires already occupied or that it fails to be detected reaching one of the $N-n$ unoccupied nanowires. The second term is the probability that $n-1$ photons are detected when $m-1$ are sent times the probability that the mth photon reaches one of the $N-n+1$ unoccupied nanowires and it is detected. In the limit $\eta_i = \eta$ for $i = 1, \ldots, N$, the recursion relation agrees with that given in ref. 14.

DETECTION PROBABILITIES UNDER WEAK LASER ILLUMINATION

In the case of laser illumination, as used in the reported experiments, the photon number distribution is close to a poissonian $S(m) = \mu^m \exp(-\mu)/m!$ (μ, mean photon number). The limited efficiency $\eta < 1$ of the detector is equivalent to an optical loss, and reduces the mean photon number to $\tilde{\mu} = \eta\mu$. In the regime $\tilde{\mu} \ll 1$, $S(m) \sim \tilde{\mu}^m/m!$, and for $\tilde{\mu}$ low enough the measured distribution can be written as

$$Q(n) \sim P(n|n) \cdot S(n) \propto \tilde{\mu}^n/n! \qquad \text{for } \tilde{\mu} \ll 1 \tag{4}$$

Received 5 November 2007; accepted 13 February 2008; published 13 April 2008.

References

1. Simon, C. *et al.* Quantum repeaters with photon pair sources and multimode memories. *Phys. Rev. Lett.* **98,** 190503 (2007).
2. Knill, E., Laflamme, R. & Milburn, G. J. A scheme for efficient quantum computation with linear optics. *Nature* **409,** 46–52 (2001).
3. Fujiwara, M. & Sasaki, M. Direct measurement of photon number statistics at telecom wavelengths using a charge integration photon detector. *Appl. Opt.* **46,** 3069–3074 (2007).
4. Gansen, E. J. *et al.* Photon-number-discriminating detection using a quantum-dot, optically gated, field-effect transistor. *Nature Photon.* **1,** 585–588 (2007).
5. Kardynal, B. E. *et al.* Photon number resolving detector based on a quantum dot field effect transistor. *Appl. Phys. Lett.* **90,** 181114 (2007).
6. Rosenberg, D., Lita, A. E., Miller, A. J. & Nam, S. W. Noise-free high-efficiency photon-number-resolving detectors. *Phys. Rev. A* **71,** 1–4 (2005).
7. Zambra, G. *et al.* Counting photoelectrons in the response of a photomultiplier tube to single picosecond light pulses. *Rev. Sci. Instrum.* **75,** 2762–2765 (2004).
8. Waks, E. *et al.* High-efficiency photon-number detection for quantum information processing. *IEEE J. Sel. Top. Quant.* **9,** 1502–1511 (2003).
9. Waks, E. *et al.* Direct observation of nonclassical photon statistics in parametric down-conversion. *Phys. Rev. Lett.* **92,** 113602 (2004).
10. Yamamoto, K. *et al.* Development of multi-pixel photon counter (MPPC). *IEEE Nucl. Sci. Symp. Conf. Record 2006* **2,** 1094–1097 (2006).
11. Jiang, L. A., Dauler, E. A. & Chang, J. T. Photon-number-resolving detector with 10 bits of resolution. *Phys. Rev. A* **75,** 62325 (2007).
12. Achilles, D. *et al.* Fiber-assisted detection with photon number resolution. *Opt. Lett.* **28,** 2387–2389 (2003).
13. Fitch, M. J., Jacobs, B. C., Pittman, T. B. & Franson, J. D. Photon-number resolution using time-multiplexed single-photon detectors. *Phys. Rev. A* **68,** 043814 (2003).
14. Dauler, E. A. *et al.* Multi-element superconducting nanowire single-photon detector. *IEEE Trans. Appl. Superconductivity* **17,** 279–284 (2007).
15. Gol'tsman, G. N. *et al.* Picosecond superconducting single-photon optical detector. *Appl. Phys. Lett.* **79,** 705–707 (2001).
16. Kerman, A. J. *et al.* Kinetic-inductance-limited reset time of superconducting nanowire photon counters. *Appl. Phys. Lett.* **88,** 111116 (2006).
17. Mattioli, F. *et al.* Electrical characterization of superconducting single-photon detectors. *J. Appl. Phys.* **101,** 054302 (2007).
18. Gol'tsman, G. N. *et al.* Fabrication of nanostructured superconducting single-photon detectors. *IEEE Trans. Appl. Superconductivity* **13,** 192–195 (2003).
19. Gol'tsman, G. *et al.* Middle-infrared to visible-light ultrafast superconducting single-photon detectors. *IEEE Trans. Appl. Superconductivity* **17,** 246–251 (2007).
20. Korneev, A. *et al.* Sensitivity and gigahertz counting performance of NbN superconducting single-photon detectors. *Appl. Phys. Lett.* **84,** 5338–5340 (2004).
21. Lee, H. *et al.* Towards photostatistics from photon-number discriminating detectors. *J. Modern Opt.* **51,** 1517–1528 (2004).
22. Rosfjord, K. M. *et al.* Nanowire single-photon detector with an integrated optical cavity and anti-reflection coating. *Opt. Express* **14,** 527–534 (2006).
23. McIntyre, R. J. Multiplication noise in uniform avalanche diodes. *IEEE Trans Electron. Dev.* **13,** 164–168 (1966).
24. Semenov, A. D., Gol'tsman, G. N. & Korneev, A. A. Quantum detection by current carrying superconducting film. *Physica C* **351,** 349–356 (2001).
25. Miller, A. J., Nam, S. W., Martinis, J. M. & Sergienko, A. V. Demonstration of a low-noise near-infrared photon counter with multiphoton discrimination. *Appl. Phys. Lett.* **83,** 791–793 (2003).

Acknowledgements

This work was supported by the Swiss National Foundation through the "Professeur boursier' and NCCR Quantum Photonics programs, EU FP6 STREP 'SINPHONIA' (contract no. NMP4-CT-2005-16433), EU FP6 IP 'QAP' (contract no. 15848), the grant 'Non-equilibrium processes after IR photon absorption in thin-film superconducting nanostructures' from the Russian Agency on Education and grant no. 02.445.11.7434 from the Russian Ministry of Education and Science for support of leading scientific schools. The authors thank B. Deveaud-Plédran, B. Dwir and H. Jotterand for useful discussion and technical support and the Interdisciplinary Centre for Electron Microscopy (CIME) for supplying TEM and SEM facilities. A.G. gratefully acknowledges a PhD fellowship at University of Roma TRE.

Author information

Reprints and permission information is available online at http://npg.nature.com/reprintsandpermissions/. Correspondence and requests for materials should be addressed to F.M.